Engineering Composite Oxide SOFC Anodes for Efficient Oxidation of Methane

G. Kim,[a] G. Corre,[b] J. T. S. Irvine,[b,*] J. M. Vohs,[a] and R. J. Gorte[a,*,z]

[a]*Department of Chemical and Biomolecular Engineering, University of Pennsylvania, Philadelphia, Pennsylvania 19104, USA*
[b]*School of Chemistry, University of St. Andrews, Fife KY16 9ST, Scotland*

Ceramic anodes for solid oxide fuel cells (SOFCs) were prepared by aqueous impregnation of nitrate salts to produce composites with 45 wt % $La_{0.8}Sr_{0.2}Cr_{0.5}Mn_{0.5}O_3$ (LSCM) in a 65% porous yttria-stabilized zirconia (YSZ) scaffold. Scanning electron micrographs indicate that the LSCM coats the YSZ pores following calcination at 1473 K. Composites produced in this manner exhibit conductivities at 1073 K of approximately 1 S/cm in air and 0.1 S/cm in humidified H_2. A SOFC with a composite anode composed of 45 wt % LSCM, 0.5 wt % Pd, and 5 wt % ceria exhibited maximum power densities at 1073 K of 1.1 and 0.71 W cm^{-2} in humidified (3% H_2O) H_2 and methane, respectively.
© 2007 The Electrochemical Society. [DOI: 10.1149/1.2817809] All rights reserved.

Solid oxide fuel cells (SOFCs) offer uniquely scalable, high-efficiency conversion of chemical-to-electrical energy. Present SOFC anodes based upon Ni cermets provide good electrochemical and catalytic performance but suffer from important limitations. While state-of-the-art, Ni-based anodes perform well in hydrogen-based fuels, the strong tendency of Ni to catalyze formation of carbon filaments makes SOFC operation with hydrocarbons other than methane (and even methane must be co-fed with large amounts of steam) impractical.[1] Not only is the Ni surface deactivated by surface carbon formation, but filamentous carbon can lead to loss of the Ni by metal dusting[2,3] and catastrophic fracture of Ni composites by expansion of the carbon filaments.[4] Furthermore, even the best-engineered Ni-based electrodes have only limited tolerance to oxidation during start-up and shut-down cycles due to the expansion that occurs when Ni forms NiO.[5]

Conductive ceramics would offer an attractive alternative to Ni composites if comparable electrochemical performance could be achieved.[6] Ceramic materials tend to be stable against carbon-fiber formation in hydrocarbon fuels and would be less sensitive to oxidation and reduction cycles. For operation with hydrocarbon fuels, the ability to oxidize the anode would be particularly useful, because this would allow periodic oxidation cycles to remove impurities brought in with the fuel or carbon deposits formed by gas-phase pyrolysis.[7] Because many ceramics have high melting temperatures, excellent thermal stability is also anticipated.

Our laboratories have investigated two different approaches for the development of ceramic anodes. The group at St. Andrews has been investigating oxides that show high conductivities under reducing conditions,[8,9] an effort that has demonstrated the promising properties of Sr-doped $LaCr_{0.5}Mn_{0.5}O_3$ (LSCM).[9] However, the catalytic performance of LSCM-based electrodes is not comparable to Ni-based anodes at lower temperatures.[10] The group at Penn has investigated ceramic anodes prepared by impregnation of electronically conductive and catalytic components into porous scaffolds.[11,12] The best performance was achieved by preparing thin functional layers of porous yttria-stabilized zirconia (YSZ), into which ceria and dopant levels of Pd were added for electronic conductivity and catalytic activity. While the initial performance of these anodes were excellent (the anode impedance for one cell was estimated to be 0.26 Ω cm^2 at 973 K in humidified H_2[11]), the conductivity achieved by impregnating ceria into the porous YSZ layer was not thermally stable.[12]

In the present study, we have combined these approaches by preparing LSCM-based electrodes using the porous-scaffold ap-proach. We demonstrate that high performance can be achieved in this way. The electrodes are also redox tolerant and stable in dry methane.

Experimental

Cells were fabricated by first preparing a three-layer YSZ wafer with two porous layers separated by a 65 μm thick dense electrolyte layer, as previously described.[12] The three-layer ceramic wafers were produced by laminating three green ceramic tapes, synthesized by tape casting, with pore formers in the two outer tapes. The laminated, green tapes were fired to 1773 K to produce the final ceramic structures. The porous layer on one side of the electrolyte was 300 μm thick YSZ ($\sim$65% porous) and was used as the scaffold for the cathodes, while the other porous layer was 60 μm thick YSZ ($\sim$65% porous) and was used as the scaffold for the anode. Porosity in the 300 μm layer was obtained using a mixture of graphite and polystyrene pore formers (used to introduce larger pores), while the thinner porous layer used only graphite.

After synthesizing the three-layer YSZ wafer, 45 wt % LSCM was added to the porous anode layer using an aqueous nitrate solution. The impregnating solution was prepared by adding $La(NO_3)_3 \cdot 6H_2O$ (Alfa Aesar, ACS 99.9%), $Sr(NO_3)_2$ (Alfa Aesar, ACS 99.0%), $Cr(NO_3)_3 \cdot 9H_2O$ (Alfa Aesar, ACS 98.5%), and $Mn(NO_3)_2 \cdot 4H_2O$ (Alfa Aesar, ACS 99.98%) to distilled water in the correct molar ratios, then mixing this with citric acid ($\geq$99.5%, Aldrich) to produce a solution with a citric acid/metal-ion ratio of 2:1. After infiltrating the porous layer with this solution, the ceramic wafer was heated in air to 750 K to decompose the nitrate ions and the citric acid. This procedure was repeated until the desired weight loading of LSCM was achieved. Finally, the wafer was heated in air to 1473 K for a few hours to produce the perovskite structure. Figure 1 is a diffraction pattern of the LSCM–YSZ composite formed in this way and demonstrates that the composite has the proper structure.

The electronic conductivities of the LSCM–YSZ composites were measured as a function of temperature in air and in humidified (3% H_2O) H_2 using standard, four-probe measurements on samples that were prepared by adding LSCM to porous YSZ slabs that were $1 \times 1 \times 10$ mm in size. The YSZ slabs were prepared from the same slurries used in tape casting the porous anode layers.

After forming the LSCM in the anode layer, the $La_{0.8}Sr_{0.2}FeO_3$ (LSF)–YSZ cathodes were synthesized by impregnating the 300 μm thick layer with an aqueous solution containing $La(NO_3)_3 \cdot 6H_2O$, $Sr(NO_3)_2$, and $Fe(NO_3)_3 \cdot 9H_2O$, to a loading of 40 wt % LSF, followed by calcination to 1123 K.[13,14] Detailed procedures for forming the LSF–YSZ cathodes are given elsewhere.[13] For purposes of
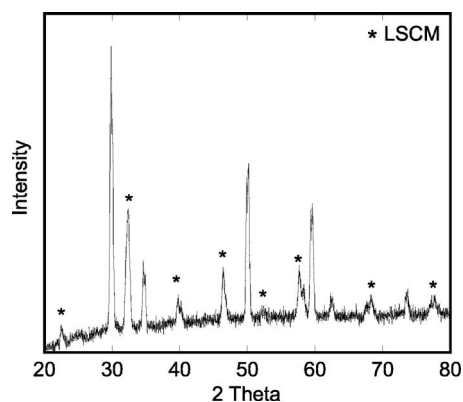
Figure 1. An XRD of an LSCM–YSZ composite with 45 wt % LSCM, formed by infiltration into porous YSZ.

(a)

(b)

(c)

Figure 2. (a) SEM image of the three-layer structure used in making the SOFC in this paper. The top layer is the porous YSZ with 45 wt % LSCM. (b) A high-resolution SEM image of the LSCM–YSZ composite with 45 wt % LSCM. (c) A high-resolution SEM image of the porous YSZ prior to the addition of LSCM.

the present study, it is only important that the impedance of LSF–YSZ cathodes prepared in this way is between 0.1 and 0.15 Ω cm^2 at 973 K and is independent of current density.[14]

Following the addition of LSF, Pd and ceria were added as catalysts to the anode layer in some of the cells by addition of aqueous solutions of the nitrate salts and heating in air to 750 K. Because 5 wt % ceria is insufficient to provide significant electronic conductivity,[12] essentially all of the electronic conductivity in the anode layers came from LSCM, whether the Pd–ceria catalyst was added or not.
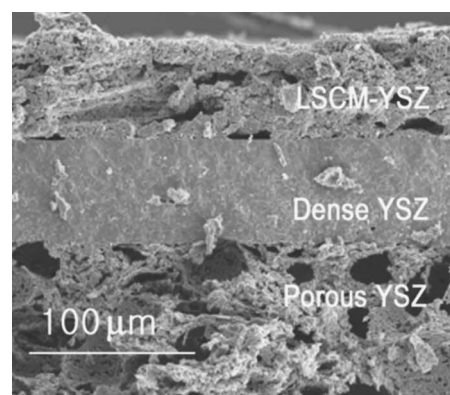
For fuel cell testing, cells were attached to an alumina tube with a ceramic adhesive (Aremco, Ceramabond 552). Electrical connections were achieved using Ag paste and Ag wire at both the anode and cathode. The fuel to the anode was either humidified (3% H$_2$O) H$_2$ or CH$_4$, while the cathode was exposed to air. Impedance spectra were measured at open circuit in the galvanostatic mode with a frequency range of 0.1 Hz to 100 kHz and a 5 mV ac perturbation using a Gamry Instruments potentiostat. The active area of the cells, equal to the anode area, was 0.35 cm^2, but the area of the electrolyte and cathode were approximately 1 cm^2.
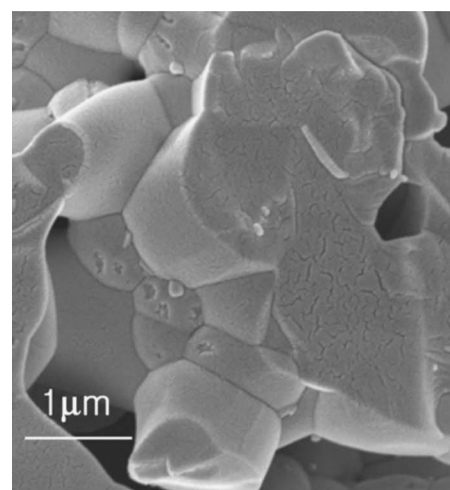
Results and Discussion

Scanning electron microscopy (SEM) micrographs of the three-layer YSZ wafer after the addition of LSCM are shown in Fig. 2. Figure 2a provides a cross-sectional view of the three layers in the region near the electrolyte. Figures 2b and c are higher-resolution images of the LSCM–YSZ composite and the porous YSZ scaffold. A comparison of the SEM images of the structures with and without the LSCM indicates that the LSCM forms a uniform coating over the surfaces of the YSZ.

In previous studies of impregnated perovskites in YSZ scaffolds,[14,15] the perovskites formed particles that were easily distinguished from the YSZ scaffold. The observation that LSCM forms a coating on the YSZ may be related to a phenomenon that was observed with La$_{0.8}$Sr$_{0.2}$MnO$_3$ (LSM) particles on YSZ single crystals.[16,17] In the case of LSM on YSZ, minimization of the surface free energy apparently caused LSM particles to spread over the YSZ crystal to form a dense film upon calcination in air above approximately 1400 K. There would be an obvious problem if a dense film of LSCM covered the YSZ, because LSCM is not a good ionic conductor. However, in the LSM case, it was observed that the film broke up into particles under mild reducing conditions.[16,17]
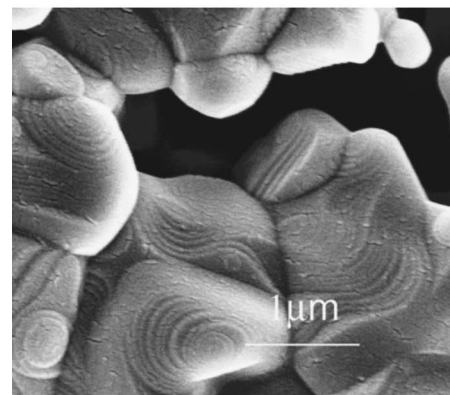
The conductivities obtained from four-probe measurements on a YSZ slab with similar porosity to the anode layer with 45 wt % LSCM added are reported in Fig. 3 as a function of temperature, in air and in humidified (3% H$_2$O) H$_2$. The conductivities of the composite are weakly temperature dependent, with values of approximately 1 S cm^{-1} in air and 0.1 S cm^{-1} in H$_2$ at 1173 K. The fact that the conductivity decreases dramatically in reducing environ-

ments is proof that the conductivity originates from the LSCM.[9] While the conductivities of the composite are significantly lower than that of the bulk LSCM, for which the reported values are 30 S cm^{-1} in air and 1–2 S cm^{-1} in H$_2$ at 1173 K,[9] they are relatively high for a composite that is only 28 vol % LSCM. This is a result of the nonrandom manner in which the composite was formed and has been observed previously for composites formed by
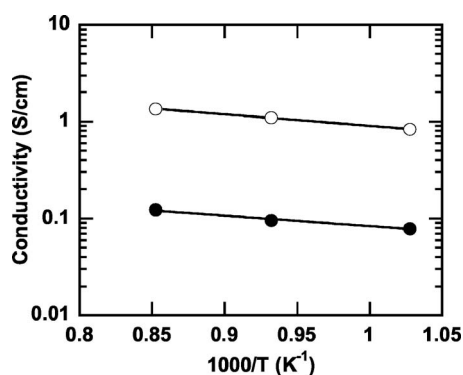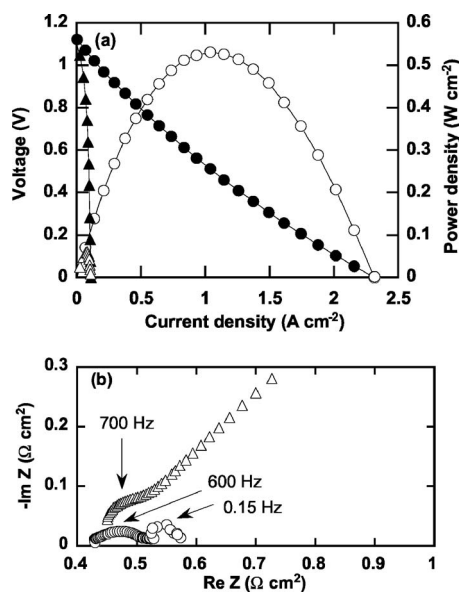
Figure 3. The electrical conductivities for the 45 wt % LSCM–YSZ composite in air (open circles) and humidified H_2 (filled circles) as a function of temperature.
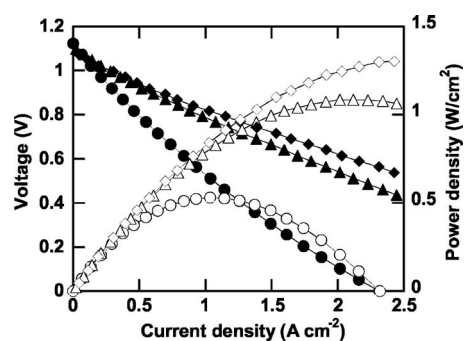

Figure 5. *V-i* polarization curves for the cell with the anode containing 0.5 wt % Pd and 5 wt % ceria, measured in humidified H_2 (3% H_2O) ($\bigcirc$) at 973, ($\triangle$) at 1073, and ($\diamond$) at 1173 K.

infiltration.[15] A conductivity of 0.1 S cm^{-1} is also sufficient for the functional layer of an electrode. The ohmic losses for a 60 μm thick electrode with this conductivity would be 0.06 Ω cm^2.

Two cells were prepared with 45 wt % LSCM in a 60 μm thick porous YSZ, and Pd and ceria were added at levels of 0.5 and 5 wt % to the anode of one of the cells. The voltage–current density (*V-i*) polarization and impedance results for these two cells are shown in Fig. 4 for operation at 973 K in humidified H_2. The open-circuit voltage was near the theoretical Nernst potential, 1.1 V, for both cells, and the *V-i* relationships were nearly linear. However, the maximum power density for the cell without Pd or ceria was less than 50 mW cm^{-2}, while the maximum power density for the cell with Pd and ceria was 520 mW cm^{-2}.

The impedance data in Fig. 4b indicate that the ohmic losses for both cells were nearly the same, 0.45 Ω cm^2 for the cell without Pd and ceria and 0.43 Ω cm^2 for the cell with Pd and ceria. These values are slightly higher than the sum of the expected ohmic losses from the 65 μm YSZ electrolyte (0.31 Ω cm^2) and the anode losses based on conductivity measurements (0.06 Ω cm^2). The big differ-

Figure 4. (a) *V-i* polarization and (b) impedance spectra for LSCM–CeO$_2$–Pd impregnated on 60 μm YSZ backbone with 45 wt % LSCM, 5 wt % ceria, and 0.5 wt % Pd in humidified H_2 (3% H_2O) at 973 K: ($\bigcirc$) with Pd/ceria and ($\triangle$) without Pd/ceria. The impedance data on the cell with Pd/ceria were taken at 150 mA/cm^2. Only the high-frequency part of the impedance curve on the cell without Pd/ceria is shown.

ence between the two cells was in the non-Ohmic losses, which were 0.14 Ω cm^2 on the cell with the added catalyst and 2.2 Ω cm^2 on the cell without. This is in accord with the previously reported high activation energy for LSCM electrode processes, although still perhaps a factor of 1.5–2 greater than might be extrapolated for a pure LSCM electrode.[9] It is instructive to consider the difference between the two impedance plots in Fig. 4b. Clearly the high-frequency part of the impedance curves is not greatly changed by addition of Pd/CeO$_2$ catalyst. This part probably relates to cathode-polarization losses as the value is similar to that previously estimated for such a cathode,[13,14] although there may also be a small contribution from electrochemical processes involving ion transport through the microstructure at the anode, which would be expected in this frequency range for LSCM.[18,19] The lower-frequency polarization arc decreases greatly with addition of Pd/CeO$_2$ and so must be associated with the anode, most probably charge transfer at the interfaces, and is consistent with previous observations in electrode-impedance studies.[18,19]

The effect of temperature on the performance in humidified H_2 of the cell with Pd and ceria is shown in Fig. 5. The maximum power density increased to 1.1 W cm^{-2} at 1073 K and 1.4 W cm^{-2} at 1173 K. Because the majority of the losses in this cell were associated with the electrolyte, even at 973 K, most of this improvement is due to a decrease in the ohmic losses.

In an earlier study which used impregnated ceria in thin electrodes to achieve conductivity, there was a significant loss in the performance at 973 K after heating to high temperatures due to a loss of conductivity in the anode.[12] However, the effects of high-temperature treatments on the LSCM-based electrode were significantly less. After heating to 1073 K for 5 h, the performance at 973 K remained unchanged. After heating to 1173 K for an additional 5 h, the maximum power density at 973 K dropped slightly from 520 to 480 W cm^{-2}. More importantly, the small loss in performance following high-temperature treatment was due to an increase in the non-Ohmic losses, probably associated with changes in the Pd/ceria catalyst. The conductivity of the electrode remained unchanged. Finally, the electrode was found to be stable after a full redox cycle.

The *V-i* polarization data for the cell with Pd–ceria catalyst in humidified (3% H_2O) CH$_4$ are shown in Fig. 6. A strong curvature in the *V-i* relationship near OCV may indicate that activation of CH$_4$ by polarization is required. Even with these losses, the maximum power densities in CH$_4$ were nearly as high as was achieved in H_2, 400 W cm^{-2} at 973 K and 710 W cm^{-2} at 1073 K. These performances in methane are remarkably good and compare well with those previously reported at 1073 K in the absence of significant steam. To our knowledge the best previous data for methane at 1073 K in low-steam conditions, in cells that are stable in the absence of current, are 550 W cm^{-2} for Pd/CeO$_2$ impregnated YSZ[11] and 400 W cm^{-2} for Sr$_2$MgMoO$_6$.[20] Different studies on
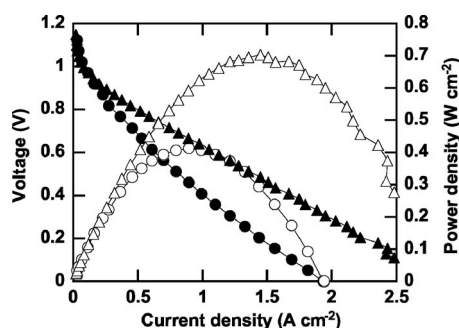
Figure 6. *V-i* polarization curves for the cell with the anode containing 0.5 wt % Pd and 5 wt % ceria, measured in humidified (3% H_2O) CH_4 at (○) at 973 and (△) at 1073 K.

(Gd, Ce)O_{2-x} nanoparticle impregnated LSCM have achieved 158 W cm^{-2} power output and 0.44 Ω cm^2 polarization resistance at 1073 K in humidified methane.[21,22]

It is important to recognize that the anode compositions used in the present study are not the only factor leading to the significantly improved electrode performance. Structure is clearly critical. Impregnation procedures allow much more control over this structure than normal ceramics processing methods. In the present case, it appears that advantageous surface interactions between LSCM and YSZ also assist in forming a good electrode structure. Clearly, this is an issue worthy of future study.

Conclusion

We have demonstrated the capability of liquid-phase impregnation and in situ sintering to engineer a highly effective nanocomposite SOFC anode that exhibits excellent performance in both H_2 and CH_4 and is thermally and chemically robust.

References

1. S. McIntosh and R. J. Gorte, *Chem. Rev. (Washington, D.C.)*, **104**, 4845 (2004).
2. M. L. Toebes, J. H. Bitter, A. J. van Dillen, and K. P. de Jong, *Catal. Today*, **76**, 33 (2002).
3. C. H. Toh, P. R. Munroe, D. J. Young, and K. Foger, *Mater. High. Temp.*, **20**, 129 (2003).
4. H. Kim, C. Lu, W. L. Worrell, J. M. Vohs, and R. J. Gorte, *J. Electrochem. Soc.*, **149**, A247 (2002).
5. M. Cassidy, G. Lindsay, and K. Kendall, *J. Power Sources*, **61**, 189 (1996).
6. A. Atkinson, S. Barnett, R. J. Gorte, J. T. S. Irvine, A. J. McEvoy, M. Mogensen, S. Singhal, and J. Vohs, *Nat. Mater.*, **3**, 17 (2004).
7. T. Kim, G. Liu, M. Boaro, S. I. Lee, J. M. Vohs, R. J. Gorte, O. H. Al-Madhi, and B. O. Dabbousi, *J. Power Sources*, **155**, 231 (2006).
8. J. C. Ruiz-Morales, J. Canales-Vasquez, C. Savaniu, D. Marrero-Lopez, W. Zhou, and J. T. S. Irvine, *Nature (London)*, **439**, 568 (2006).
9. S. W. Tao and J. T. S. Irvine, *J. Electrochem. Soc.*, **151**, A252 (2004).
10. S. W. Tao, J. T. S. Irvine, and S. M. Plint, *J. Phys. Chem.*, **110**, 21771 (2006).
11. M. D. Gross, J. M. Vohs, and R. J. Gorte, *Electrochem. Solid-State Lett.*, **10**, B65 (2007).
12. M. D. Gross, J. M. Vohs, and R. J. Gorte, *J. Electrochem. Soc.*, **154**, B694 (2007).
13. Y. Huang, J. M. Vohs, and R. J. Gorte, *J. Electrochem. Soc.*, **151**, A646 (2004).
14. W. S. Wang, M. D. Gross, J. M. Vohs, and R. J. Gorte, *J. Electrochem. Soc.*, **154**, B439 (2007).
15. H. P. He, Y. Y. Huang, J. Regal, M. Boaro, J. M. Vohs, and R. J. Gorte, *J. Am. Ceram. Soc.*, **87**, 331 (2004).
16. Y. Huang, J. M. Vohs, and R. J. Gorte, *J. Electrochem. Soc.*, **152**, A1347 (2005).
17. Y. Huang, J. M. Vohs, and R. J. Gorte, *Electrochem. Solid-State Lett.*, **9**, A237 (2006).
18. D. M. Bastidas, S. W. Tao, and J. T. S. Irvine, *J. Mater. Chem.*, **16**, 1603 (2006).
19. M. J. Jorgensen and M. Mogensen, *J. Electrochem. Soc.*, **148**, A433 (2001).
20. Y. H. Huang, R. I. Dass, Z. L. Xing, and J. B. Goodenough, *Science*, **312**, 254 (2006).
21. X. J. Chen, Q. L. Liu, S. H. Chan, N. P. Brandon, and K. A. Khor, *Electrochem. Commun.*, **9**, 767 (2007).
22. S. P. Jiang, X. J. Chen, S. H. Chan, and J. T. Kwok, *J. Electrochem. Soc.*, **153**, A850 (2006).